Journal of Power Sources 196 (2011) 3239–3243

Contents lists available at ScienceDirect

Journal of Power Sources

journal homepage: www.elsevier.com/locate/jpowsour

Short communication

Flexible thermoelectric generator for ambient assisted living wearable biometric sensors

L. Francioso[a,*], C. De Pascali[a], I. Farella[a], C. Martucci[a], P. Cretì[a], P. Siciliano[a], A. Perrone[b]

[a] CNR-IMM, Institute for Microelectronics and Microsystems, Lecce, Italy
[b] University of Salento, Faculty of Engineering, Lecce, Italy

ARTICLE INFO

Article history:
Received 20 July 2010
Received in revised form
11 November 2010
Accepted 18 November 2010
Available online 24 November 2010

Keywords:
Thermoelectric
Flexible generator
Ambient assisted living
Wearable

ABSTRACT

In this work we proposed design, fabrication and functional characterization of a very low cost energy autonomous, maintenance free, flexible and wearable micro thermoelectric generator (μTEG), finalized to power very low consumption electronics ambient assisted living (AAL) applications. The prototype, integrating an array of 100 thin films thermocouples of Sb_2Te_3 and Bi_2Te_3, generates, at 40 °C, an open circuit output voltage of 430 mV and an electrical output power up to 32 nW with matched load. In real operation conditions of prototype, which are believed to be very close to a thermal gradient of 15 °C, the device generates an open circuit output voltage of about 160 mV, with an electrical output power up to 4.18 nW.

In the first part of work, deposition investigation Sb_2Te_3 and Bi_2Te_3 thin films alloys on Kapton HN polyimide foil by RF magnetron co-sputtering technique is discussed. Deposition parameters have been optimized to gain perfect stoichiometric ratio and high thermoelectric power factor; fabricated thermogenerator has been tested at low gradient conditioned to evaluate applications like human skin wearable power generator for ambient assisted living applications.

1. Introduction

In the framework of European ambient assisted living (AAL) program for increasing the quality of life of older people using pervasive information and communication technology (ICT) infrastructure, the interest of scientific community and caregivers for low cost solutions for wearable biometric monitoring sensors, energy autonomous and maintenance free has grown very fast during the last years. State-of-the art monitoring nodes are typically powered by rechargeable batteries, with known drawbacks for continuous operation from elderly peoples or human beings affected by cognitive diseases. In order to extending the life-time of traditional batteries, intensive research is currently focused on the development of portable power generators able to harvest energy from environmental sources and convert it into electricity. Furthermore, the technological transfer of such microsystems on flexible substrates is the key point for the development of unobtrusive low cost wearable and ubiquitous integrated devices for healthcare and biometric parameters monitoring.

The conversion between thermal and electrical energy by thermoelectric effect is one of the simplest process through which perform energy scavenging (extraction/reconversion of the energy) from heat sources.

Thermoelectric materials are solid-state conductors or semiconductors that directly produce a temperature gradient from an applied voltage (Peltier effect) or transform thermal energy from a temperature gradient into electrical energy (Seebeck effect). A thermoelectric converter has the advantage of no moving mechanical parts (like piezoelectric scavengers), useful for integration on flexible modules.

The voltage, or thermoelectric electromotive force (EMF), produced by Seebeck effect is defined as:

$$V = (\alpha_a - \alpha_b)\Delta T = \alpha_{ab}\Delta T \quad (1)$$

where α_{ab} indicates the relative Seebeck coefficient for the material pair *a*–*b*.

The thermoelectric conversion efficiency of a material is directly related to the dimensionless parameter figure of merit (*ZT*), defined as:

$$ZT = \frac{\alpha^2\sigma}{\lambda}T \quad (2)$$

where α is the above mentioned relative Seebeck coefficient, σ is the electrical conductivity, λ is the thermal conductivity (as sum of contributions from electronic carriers and lattice) and *T* is the absolute temperature.

* Corresponding author. Tel.: +39 0832422525; fax: +39 0832422552.
E-mail address: luca.francioso@le.imm.cnr.it (L. Francioso).

0378-7753/$ – see front matter © 2010 Elsevier B.V. All rights reserved.
doi:10.1016/j.jpowsour.2010.11.081

Therefore thermal, electrical and semiconductor properties of active materials are fundamental for design and enhanced performances operation of thermoelectric devices.

In order to maximize the generated output voltage, several thermocouples are connected electrically in series each other and thermally in parallel to form a thermopile, which is able to generate n times the output voltage of one thermocouple (if n is the number of thermocouples in series) and a maximum output electric power (with optimal impedance matching) given by

$$P_{MAX} = \frac{(n\alpha_{ab}\Delta T)^2}{4R_0} \quad (3)$$

where R_0 internal electrical resistance of generator

By far the most widely used thermoelectric materials are Bi_2Te_3 and Sb_2Te_3 because of their high thermoelectric efficiency near to room temperature and different deposition methods have been reported for such materials as thin films. Thermal co-evaporation [1], DC or RF co-sputtering [2–5], electrochemical deposition [6], flash evaporation [7] are some examples.

In this work, high quality and uniformity p-Sb_2Te_3 and n-Bi_2Te_3 thin films were deposited thanks to the high level of process control and purity of adopted co-sputtering technique; Kapton substrate has been chosen because of its good thermal properties and superior temperature resistance. As well, the use of a flexible substrate is a winning strategy in wearable bending applications, such as integrated microsystems for healthcare and biometric parameters monitoring. The scientific community investigation on this field is recently increased, because of growing need of miniaturized power sources and wearable requirement; one of the innovative aspect of this work is that all fabrication steps are performed implementing high resolution UV lithography and lift-off steps, avoiding wet etching procedures [8] with limited integration capabilities and materials compatibility.

The thin films deposition process has been optimized to achieve stoichiometric ratio of compounds and high thermoelectric power factor; structural and electrical properties of TE materials as function of annealing temperature were investigated by X-ray diffraction analysis and Van der Pauw method. Starting from optimized deposition parameters obtained in the first part of work, a flexible μTEG realized and its preliminary electrical characterization reported.

2. Materials and methods

2.1. Sb_2Te_3/Bi_2Te_3 thin films deposition

50 μm-thick Kapton substrate was ultrasonically cleaned in acetone for 5 min before deposition, then washed in deionized water, dried and baked to 110 °C for 10 min, in order to remove organic residuals. High purity bismuth (99.999%), antimony (99.555%) and tellurium (99.555%) 4″ targets were used for the deposition of n-type and p-type films by RF magnetron co-sputtering.

One of the challenging issues regarding design and fabrication of thermoelectric generators concerns the deposition of films with exact compositional stoichiometry, which influence on final thermoelectric properties of materials is well known.

As regards bismuth–antimony–telluride based thin films, because of the large difference in the vapour pressures of bismuth and antimony with respect to that of tellurium, controlling the stoichiometric composition is difficult and chemical compositional gradient along the film thickness can result if a not appropriate deposition method is used. In order to obtain best stoichiometric ratio of compounds, we carried out high resolution weight and thickness measurements to optimize the co-sputtering process of the two alloys. Table 1 reports the weight percentage composition of the elements in both thin films co-sputtered under optimal deposition parameters [1].

Table 1
Composition analysis of two thin films grown at the optimal parameter.

Film type	Element (wt.%)	Expected (wt.%)
p-Sb_2Te_3	(Sb)39 ± 0.5 (Te)61 ± 0.5	(Sb)39.0 ± 0.5 (Te)61.0 ± 0.5
n-Bi_2Te_3	(Bi)50 ± 0.5 (Te)50 ± 0.5	(Bi)52.5 ± 1.0 (Te)47.5 ± 1.0

Total argon flow during deposition has been set to 25 sccm and chamber pressure was about 7.9×10^{-3} mbar. Bi_2Te_3 films were prepared powering bismuth and tellurium targets with 25 W and 30 W, respectively. 30 W RF power was applied to both targets for deposition of Sb_2Te_3 films; all deposited p-type and n-type thin films were 500 nm thick. The subsequent thermal treatment of samples was performed in a conventional tubular oven under nitrogen gas flow (5 l min^{-1}, 2 bar) with a heating rate of 5 °C min^{-1} for 1 h at 3 different temperatures, 175 °C, 225 °C and 275 °C.

X-ray diffraction analysis and Van der Pauw measurements (electrical resistivity, carrier concentration and Hall mobility) were carried out on as-deposited and annealed films, in order to select the best thermal treatment.

2.2. μTEG design and fabrication

The conversion efficiency of a thermoelectric generator is strongly affected by both electrical and thermal properties and geometric cross-sectional areas of the thermocouple legs. It has been shown [9] that optimal design occurs when following relation is satisfied

$$\frac{A_n}{A_p} = \sqrt{\frac{\lambda_p \rho_n}{\lambda_n \rho_p}} \quad (4)$$

where A_n and A_p are the geometric cross-sectional areas of the n-type and p-type thermolegs, respectively.

Using typical material properties given in Table 2 [5,10,11], an optimum ratio was calculated to be $A_n/A_p = 1.69$. As both co-sputtered thin film alloys are 500 nm thick, the above-mentioned ratio was only determined by the proportionality between L_3 and L_4.

For the photolithographic steps of fabrication run, thin acetate sheets were used as flexible masks. Therefore the dimensioning of the thermoelectric prototype was carried out as function of the minimum feature dimension obtainable with these cheap masks, about 250 μm.

Main geometrical details are shown in Fig. 1.

The internal resistance R_0 of the single thermocouple can be calculated by [2]:

$$R_0 = \frac{1}{\sigma_p}\frac{L_1 + L_5}{L_3 T_f} + \frac{1}{\sigma_n}\frac{L_1 + L_5}{L_4 T_f} + \frac{1}{\sigma_{Au}}\frac{L_2 - (L_3 + L_4)}{L_5 T_f} \quad (5)$$

where σ_p and σ_n are electrical conductivity of p- and n-type material respectively, σ_{Au} is the electrical conductivity of gold and T_f is the thickness of TE materials. Adopting relation (5), the calculated value of generator internal resistance is about 43.5 KΩ, since 100 thermocouples were integrated in the array.

The fabrication process of the prototype required three mask levels, two for active materials deposition and last one for gold metallization. The realized μTEG has an area of about 70×30 mm^2,

Table 2
Parameters used for calculation.

Material	α (μV K^{-1})	ρ (Ω m)	λ (W m^{-1} K^{-1})
p-Sb_2Te_3	209	1.08×10^{-5}	1.80
n-Bi_2Te_3	−200	1.97×10^{-5}	1.15

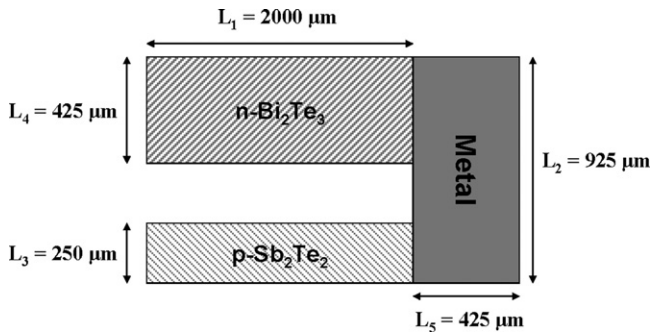

Fig. 1. A pair of p–n couple of the device, and parameters that specify the dimension of the device.

integrates 100 Sb_2Te_3/Bi_2Te_3 thermocouples and presents, at room temperature, an experimental internal resistance of about 380 KΩ; this value is higher than calculated one and can be explained by metal-semiconductor contact resistance effect (not evaluated in (5)) and reduced effective geometrical dimensions of semiconductor thin film paths due to the overlapping of gold contacts on active regions.

Comb-like gold radiators placed on cold junctions, help to improve heat dissipation and increase thermal gradient between hot and cold junctions. Different solutions have been adopted from other groups, mainly based on silicon substrate [12] with prototypes not suitable for bended surfaces or based on SU-8 mold [13], solution that required additional materials cost and preliminary processes of mold structure. Our aim is oriented to a technological solution able to be developed in the future also for complete PDMS package and direct human being skin application.

The prototype presents embedded heater and thermometer for external heating and monitoring the hot junction temperature during the electrical-functional characterization of the device. Fig. 2 reports a photograph (left) and a schematic (right) of the realized micro generator.

3. Results and discussion

The electrical characterization of the as-deposited film and annealed films was carried out at room temperature with Van der Pauw method. The bulk concentration of the Bi_2Te_3 alloy is, as expected, negative, because the material is n-type, while in Fig. 3a it has been reported in absolute value. With the increase of the post-annealing temperature, the carrier concentration decreased because of defects reduction in the polycrystalline structure.

The mobility increased in accord with the growth of the grains, and reached the maximum value of 15.10 $cm^2\ V^{-1}\ s^{-1}$ and 38.37 $cm^2\ V^{-1}\ s^{-1}$ for p- and n-type materials (Fig. 3b), respectively, at the post-annealing temperature of 275 °C. As a consequence, films conductivity ($1/\rho$), shown in Fig. 3c, also increased with the post-annealing temperature.

The SEM images in Fig. 4 reveal the morphology of p- and n-type thin films. The films were polycrystalline without preferential crystallite orientation, and visible smallest grains for antimony telluride material.

Fig. 5 reports XRD patterns of annealed $(Sb/Bi)_2Te_3$ thin films. With regard to p-type films, all the XRD pattern peaks can be well related to the hexagonal Sb_2Te_3 structure (Fig. 5a).

With regard to n-type films, some weak intensity peaks corresponding to hexagonal phase also appears in the diffractograms, but rhombohedral structure seems to be dominant. The strongest peak is related to {2 2 1} planes (Fig. 5b).

The absence of a preferential crystallite orientation reveals the polycrystalline nature of both alloys; furthermore, an evaluation of full-width at half maximum (FWHM) of diffraction lines, one can see that the grain size increases with the annealing temperature.

The post-annealing temperature of 225 °C seems to be the best annealing temperature leading to materials properties consistent with published bibliography regarding similar devices.

In order to test microgenerator performances with small temperature differences, we performed a preliminary electrical characterization of the prototype starting from 5 °C gradient up to 40 °C.

The hot junctions temperature was set by Joule effect applying a DC voltage to the heater by a digital voltage source. The effective temperature supplied by heater was determined using an ammeter, measuring the current passing thought the thermometer and calculating the corresponding value of resistance, which, as well known, changes with the temperature. As from this value, it has been possible determine the temperature of hot junctions using

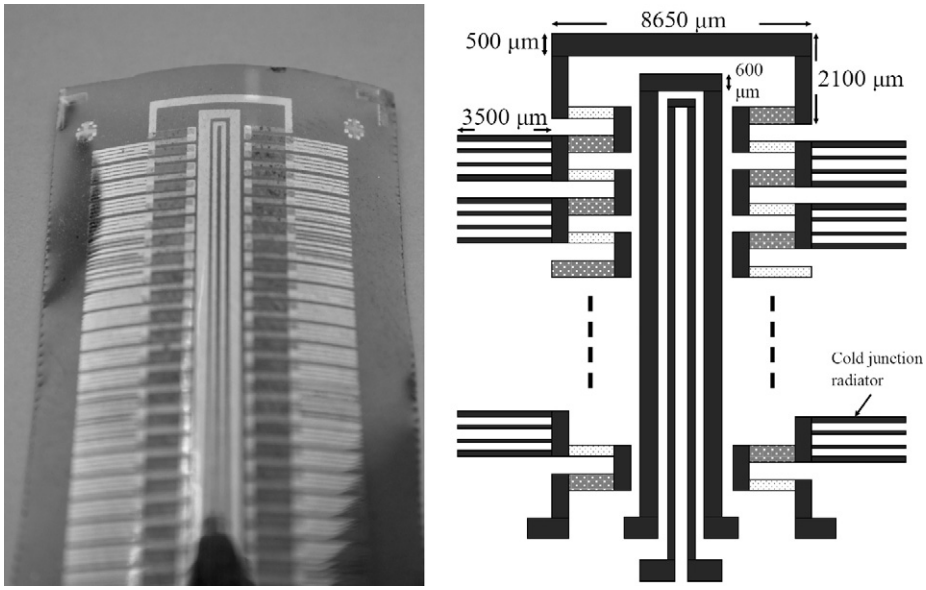

Fig. 2. (a) Photograph of fabricated flexible μTEG on Kapton HN. (b) Schematic of flexible thermoelectric generator.

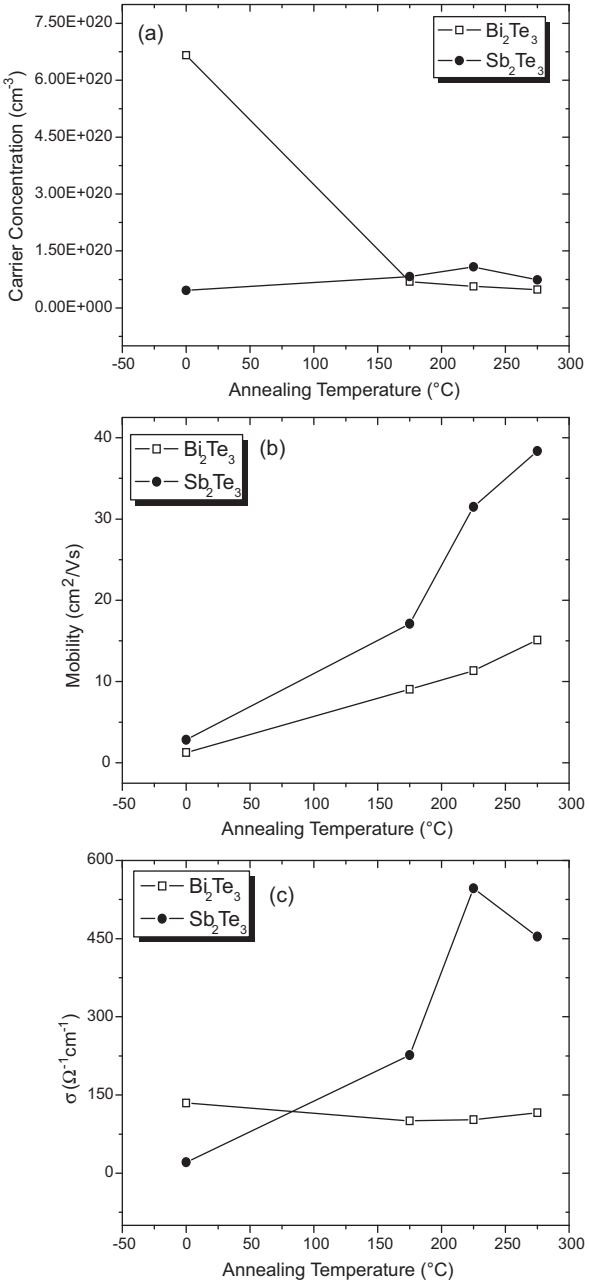

Fig. 3. Variation of semiconductor materials parameters vs. thermal annealing temperature.

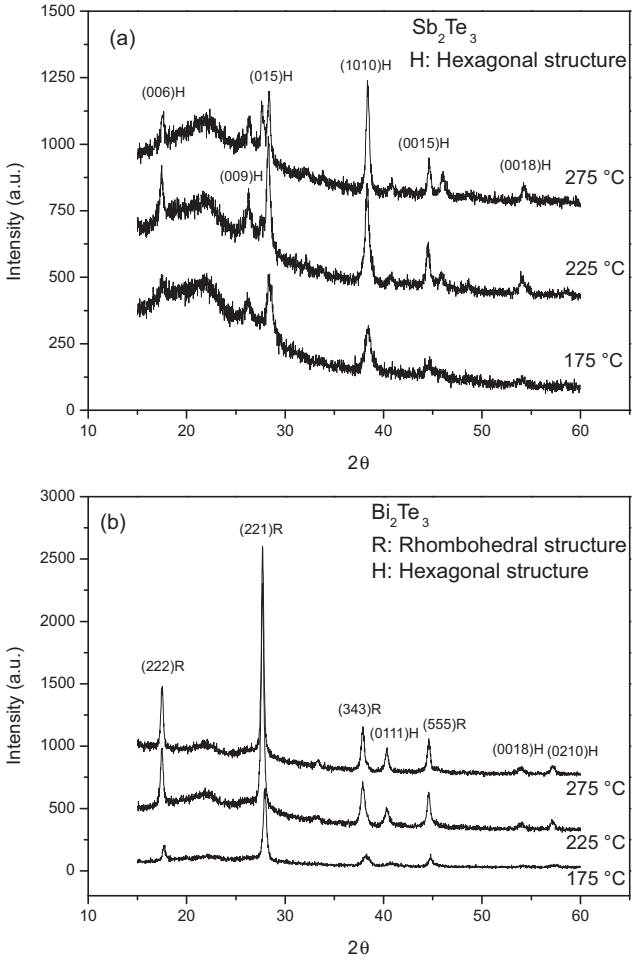

Fig. 5. X-ray diffraction analysis (XRD) of p-type (a) and n-type (b) annealed thin films.

the following relation:

$$R_T = R_{To}(1 + \alpha(T - T_o)) \quad (6)$$

where R_{To} is the thermometer resistance at room temperature (T_o) and α is the gold temperature coefficient, experimentally determined by thermometer calibration. In our case, α was about $0.00250 \pm 0.00006\,^{\circ}C^{-1}$. For different temperature gradients, the generator open circuit output voltage was measured by KEITHLEY 4200.

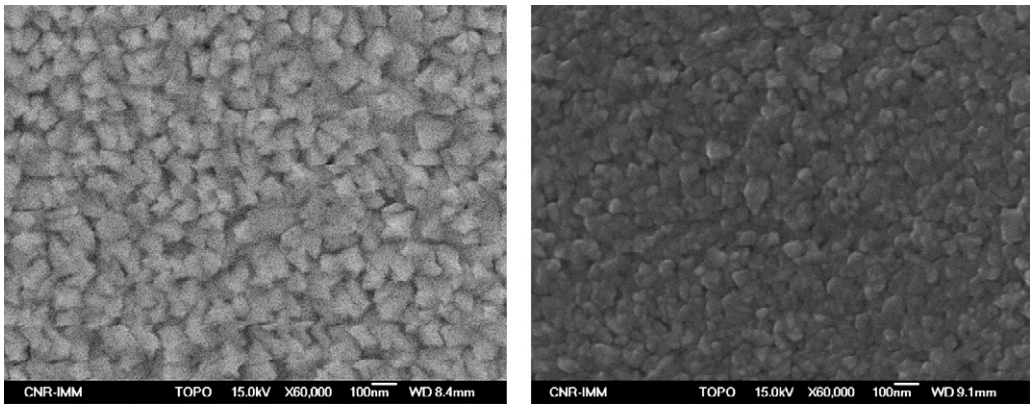

Fig. 4. SEM images of bismuth telluride (left) and antimony telluride (right) thin films deposited.

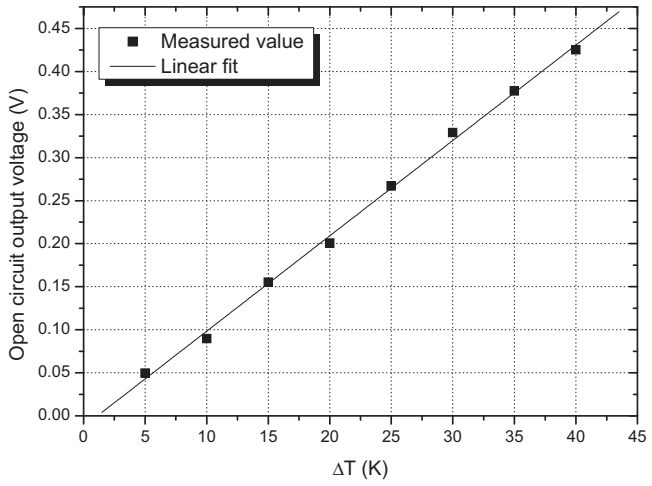

Fig. 6. Microgenerator open circuit output voltage vs. different temperature gradients.

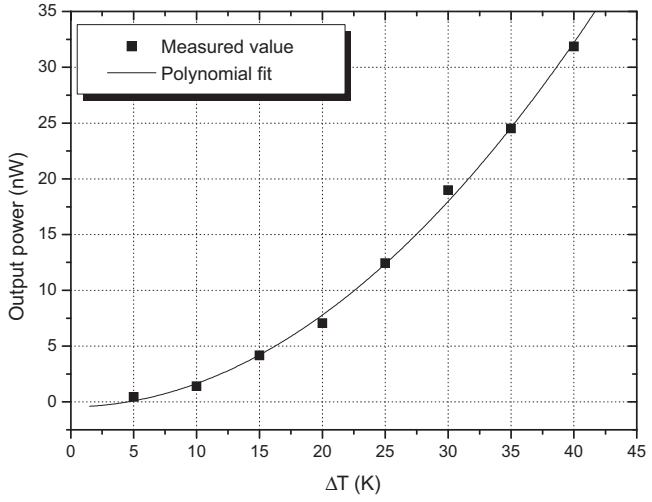

Fig. 7. Output power of the generator vs. different temperature gradients.

Figs. 6–7 show the experimental variation of the open circuit output voltage of microgenerator versus temperature difference between hot and cold junctions and the maximum generator output power, obtained for optimal impedance matching using Eq. (3).

As reported, the prototype generates, at 40 °C temperature difference, an open circuit voltage of about 430 mV, with an electrical output power up to 32 nW with optimal impedance matching.

4. Conclusions

A prototype of miniaturized thermoelectric generator with the added value of low cost flexible substrate (Kapton HN) has been designed and fabricated by microelectronics facilities; complete investigation of active materials deposition, electrical properties characterization, SEM and Van der Pauw analysis have been performed.

The reduced version of generator integrates 100 thermocouples of n- and p-type thermoelectric alloys deposited by RF co-sputtering 500 nm thick. Experimental validation of prototype has been performed for different temperature gradients, with particular attention to gradients below 15 °C for human skin wearable approach for very low power consumption electronics power source device.

The open circuit voltage and electrical power increase with increasing ΔT, and reaches maximum value of $V = 430$ mV and $P_{MAX} = 32$ nW at $\Delta T = 40$ °C. The Seebeck coefficient of each thermocouple was 108 $\mu V K^{-1}$ and the internal resistance of the device was 380 KΩ.

The proof-of-concept about compatibility of fabrication processes with substrates different than silicon was successful demonstrated.

In the future opportunity to fabricate an higher output voltage device, a standard 3 V output requirements will be obtained with about 734 thermocouples in series, and calculation find an estimated output power of about 225 μW with a temperature gradient of 10 K.

References

[1] H. Zou, D.M. Rowe, G. Min, J. Vac. Sci. Technol. A 19 (3) (2001).
[2] M. Shiozaki, S. Sugiyama, N. Watanabe, H. Ueno, K. Itoigawa, Proc. 16th IEEE Int. Conf. MEMS, 2006.
[3] D.H. Kim, E. Byon, G.-H. Lee, S. Cho, Thin Solid Films 510 (2006) 148–153.
[4] H. Böttner, J. Nurnus, A. Gavrikov, G. Kühner, M. Jeägle, C. Künzel, D. Eberhard, G. Plescher, A. Schubert, K.-H. Schlereth, J. Microelectromech. Syst. 13 (2004) 3.
[5] S. Kandasamy, D. Pachoud, A. Holland, K. Kalantar-Zadeh, G. Rosengarten, W. Wlodarski, C. Mai, J. Sci. 32 (3) (2005) 459–464.
[6] W. Glatz, S. Muntwyler, C. Hierold, Sens. Actuators A 132 (2006) 337–345.
[7] A. Foucaran, Mater. Sci. Eng. B 52 (1998) 154–161.
[8] J.P. Carmo, L.M. Goncalves, R.F. Wolffenbuttel, J. Higino Correia, Microsyst. Sens. Actuators A 161 (2010) 199–204.
[9] G.S. Nolas, J. Sharp, H.J. Goldsmid, Thermoelectrics-basic Principles and New Material Developments, Springer, Berlin, 2001.
[10] D.M. Rowe (Ed.), Thermoelectrics Handbook – Macro to Nano, Taylor & Francis, 2006.
[11] S. Kandasamy, D. Pachoud, A. Holland, K. Kalantar-zadeh, G. Rosengarten, W. Wlodarski, J. Sci. 32 (3) (2005) 459–464.
[12] T. Huesgen, P. Woias, N. Kockmann, Sens. Actuators A 145–146 (2008) 423–429.
[13] E. Schwyter, W. Glatz, L. Durrer, C. Hierold, in: DTIP 2008 Proceedings, Nice.